Digital Analytics and Robotics for Sustainable Forestry

CL4-2021-DIGITAL-EMERGING-01
Grant agreement no: 101070405

DELIVERABLE 5.3

Decision Support Systems

Due date: month 37 (September 2025)
Deliverable type: R
Lead beneficiary: WSL
Contributors: PreFor, UOXF, HEX

Dissemination Level: PUBLIC

Main authors: Justus Nögel, Markus Karppinen, Sunni Kanta Prasad Kushwaha, Clemens Blattert, Janine Schweier

1 Introduction

Common Decision Support Systems (DSSs) aim to provide forest managers with information about the development of biodiversity and ecosystem services under changing management and climate conditions, thereby highlighting particular synergies and trade-offs. Such DSSs are typically based on three main components: a database, a forest growth model, and a multi-criteria decision support analysis system [18]. The interface for integrating the improved mapping system is the database, where all spatial data is stored and subsequently processed. Thus, the availability of high quality data is the key for the efficiency and accuracy of any model. In contrast to many others, we here have the unique opportunity to attain them.

Deliverable 5.3 thus, presents the integration of high-resolution LiDAR within forestry DSSs. Two different DSSs were applied: A Central-European DSS (T5.3.1) (see section 2) and a Nordic DSS (T5.3.2) (see section 3).

2 Central-European DSS

2.1 Materials and Methods

2.1.1 Study area

For the Central-European DSS, a study area in Switzerland was selected. It is located in the municipal forest of Stein am Rhein, in the canton of Schaffhausen (Fig. 1). The Area of Interest (AOI) covers 3.7 ha area and is part of the district "Oberwald". This AOI was selected due to the forest interventions that are planned for the year 2025. Our analyses therefore aim to support the local forester in taking strategical silvicultural management decisions. The AOI is dominated by Norway spruce and silver fir species. Other important tree species include European larch, Douglas fir, and Scots pine. Currently the management target focuses on timber production.

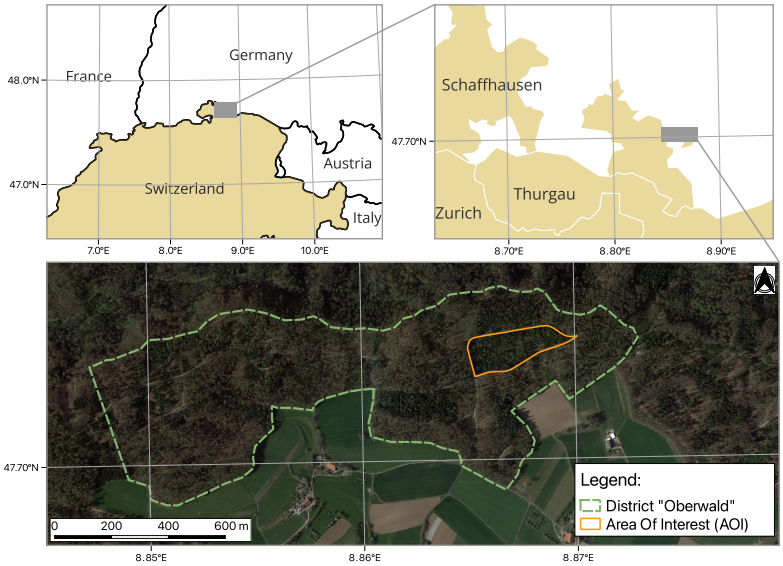

Figure 1: Switzerland study area in forest district "Oberwald" and Area of interest (AOI).

2.1.2 LiDAR Data

LiDAR data for the AOI were acquired from two different platforms, one from aerial and one from ground level i.e, Unmanned Aerial Laser Scanning (ULS) and Terrestrial Laser Scanning (TLS). The data acquisition from ULS was performed by team PreFor using a *DJI Matrice 600* UAV and *Hesai XT32-M2X* sensor during 8th - 10th July, 2024. The UAV flights were conducted at 60 m above ground level with a speed of 5 m/s with a 50 m spacing between each flight lines. For the AOI, the estimated flight time accounted to 8 minutes. The data acquisition from TLS was acquired by team HEX (Hexagon) using a *Leica RTC360* on 12th July, 10th and 14th September, 2024. A total of 473 TLS scans were acquired (Fig. 2) with a spatial resolution of 6 mm spaced at approximately 10 m from each scan positions to cover the whole AOI. The TLS acquisition was performed in total of 20.57 hours (5.56 hours/ha) and an average time of 2.61 minutes/scan. The post-processing of TLS required approximately one week and included the registration of individual scans into a complete comprehensive point cloud of the AOI. Both ULS and TLS were georeferenced as per the Swiss coordinate system (EPSG:2056) by aligning them to *swissSURFACE3D* data using an Iterative Closest Point (ICP) algorithm.

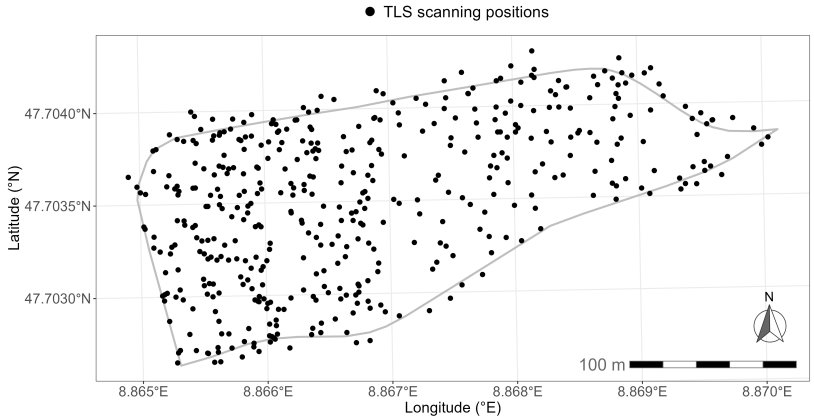

Figure 2: Spatial distribution of TLS scanning positions (n = 473).

2.1.3 LiDAR based forest inventory

Using the LiDAR data, forest inventory attributes were calculated through the following processing steps:

1. **Tiling of the point cloud**: The ULS and TLS point cloud data were divided into multiple tiles for easier data handling and processing. The tiles possess of a side lengths 26.1 m by 19.5 m.
2. **Selection of tiles for AOI:** ULS and TLS tiles were clipped, keeping only tiles within a 50 m buffer around the AOI, resulting in 115 tiles.
3. **Sub-sampling of TLS point cloud:** To reduce the size of the TLS data, each tile was sub-sampled with *CloudCompare* keeping a minimum distance between points of 2 cm.
4. **Redundant points removal:** ULS points that existed in the same voxel as TLS points were removed (voxel grid of 0.05 m) (*lidR*-package) in order to reduce the overall point density and redundancy.

5. **Fusion of ULS and TLS:** ULS possessed an average point cloud density of $1,826\ pts/m^2$ and TLS of $19,207\ pts/m^2$. The fusion of ULS and TLS data were performed using the built-in function *las_merge* of the R-package *CspStandSegmentation* [9].

6. **Re-tiling of combined tiles**: To handle overlapping tree parts across the tile boundary, a re-tiling was necessary with a buffer of 5 m. This ensures the complete segmentation of trees.

7. **Tree segmentation:** Segmentation was conducted using the platform *ForestSense* and the deep learning approach *ForAINET* [19].

8. **Removal of duplicate segmented trees:** Due to the step 6, the segmentation lead duplicates of trees. To eliminate duplicates in the buffer zone, the highest point (tree top) was taken as a decision criterion. The tree tops which were inside the initial tile boundaries were selected and the duplicate was removed.

9. **Calculation of single-tree attributes:** Based on the segmented trees, tree height, DBH, and position were derived using *CspStandSegmentation* R-package, build-in function *forest_inventory* [9].

10. **Prediction of tree species:** For tree species classification, the deep learning model *DetailView*, was applied via a python script [10, 16].

11. **Single tree error corrections:** A point cloud density raster was created (*rasterize_points*, *lidR*- package, raster cell resolution of 0.03 m, 0 - 2 m height) to visualize the spatial distribution and diameter of trees at the 2D level (Fig. 3). In *QGIS*, the derived forest inventory data was compared to the density raster and corrections were conducted: remeasuring false and missing DBH values (n = 184 trees), relocating detecting trees, removing misidentified trees and false artifacts. A DBH threshold of 7 cm was applied to filter the forest inventory, as trees below this diameter are challenging to accurately identify during segmentation, which subsequently affects the reliability of the estimated single-tree attributes [9].

12. **Tree Detection Rate (TDR):** The point density raster served as a reference to identify trees that were missed during segmentation. This enabled estimation of the total tree count for the AOI and calculation of the proportion of correctly segmented trees, defined as the Tree Detection Rate (TDR).

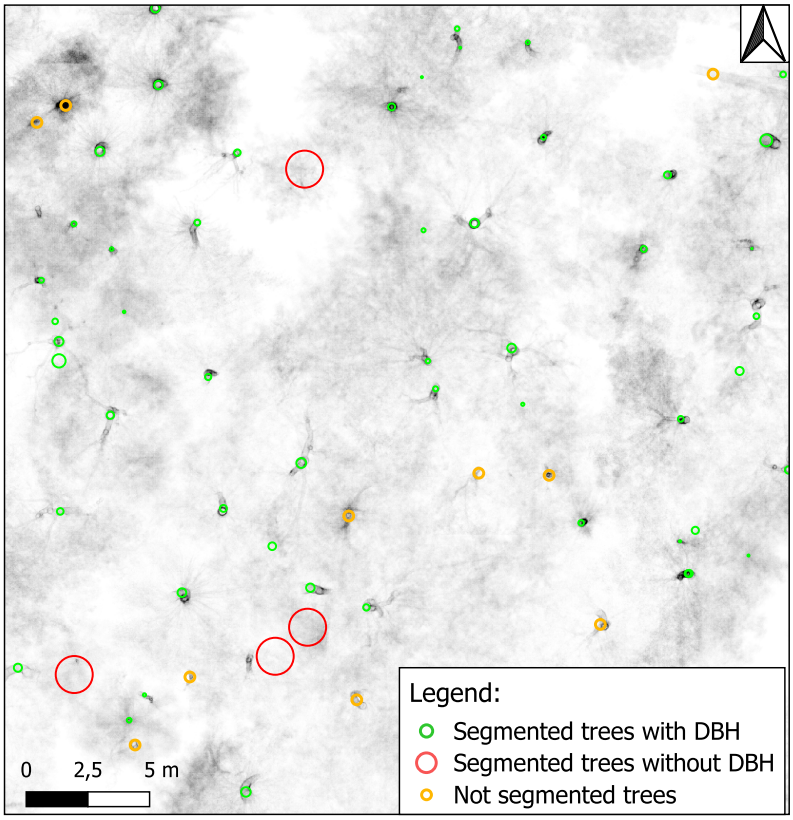

Figure 3: Single tree error corrections using point density raster layer as reference: remeasuring false and missing DBH values (n = 184 trees), relocating detecting trees, removing misidentified trees and false artifacts (based on Frey et al. [9]).

2.1.4 Forest growth simulation model: ForClim

The dynamic vegetation and gap model ForClim (v.4.1) was selected for the forest growth simulation [5, 14]. It is capable of considering climate change effects, which has been validated in various Swiss case studies, and effectively integrated within DSSs (e.g. Blattert et al. [2]). ForClim simulates key successional forest processes, such as establishment, tree growth, tree mortality, and competition, based on ecological and physiological principles. As a gap model, it follows a patch-based approach where each forest stand is divided into independent patches of 200-800 m² [4]. Within each patch, no explicit spatial positions of trees are considered, and trees of the same age and species are grouped into cohorts with identical behaviors [5]. ForClim is designed on a modular basis, with a plant, weather, water, and management submodel [4]. Recent advances were integrated within the plant submodel and the mortality processes, enhancing the model's sensitivity to drought-induced mortality [14, 8].

The initialization of ForClim V.4.1 was implemented with the following input data: (1) initial forest stand based on the LiDAR forest inventory data (see section 2.1.3), (2) management scenarios, (3) historical climate data, (4) climate change data, (5) soil data. The future forest projection was simulated from 2025 to 2095 (70 years), using the R-package *rforclim* (v. 1.01.000) [11].

(1) The forest inventory, containing tree DBH, species, height, and position data, was assigned to a grid of 400 m² patches (n = 90) (Fig. 4). Patches that were 50% or

more outside the AOI were excluded from analysis. The simulation setup incorporated all 31 parameterized tree species, enabling the model to simulate potential migration of species, which are better adapted to changing growth conditions.

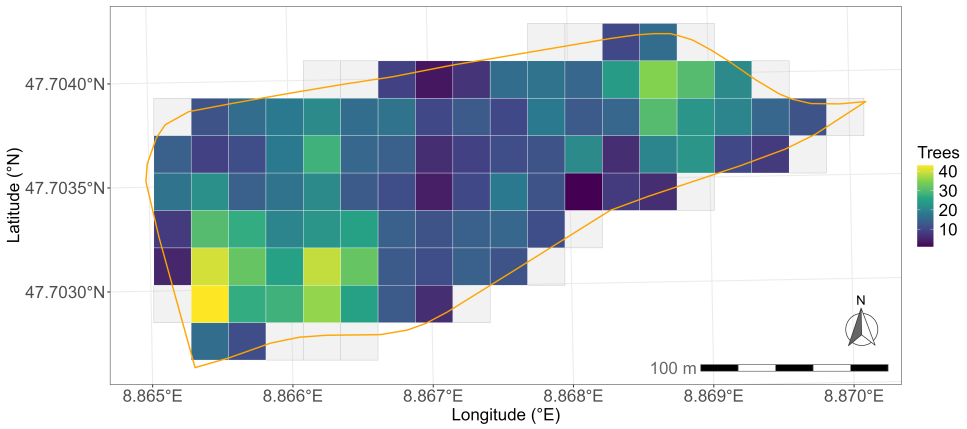

Figure 4: Spatial distribution of trees onto patches for ForClim initialization (n = 90)

(2) Three management scenarios were implemented: (i) no management interventions (NO), (ii) low-intensity plentering (LOW) with a basal area equilibrium state of 40 m^2ha^{-1}, and (iii) high-intensity plentering (HIGH) with a basal area equilibrium state of 20 m^2ha^{-1}. The plentering approach is characterized by single-tree harvesting based on targeted DBH thresholds (set to 70 cm for this study). Management cycles were conducted at 10-year intervals from 2025 to 2095.

(3) For the historical climate scenario (HIST), the reference period 1981-2010 from the Schaffhausen weather station was selected, with a mean annual temperature of 9.4°C and annual precipitation of 900 mm [15]. The HIST data was processed for the ForClim weather generator, which operates using monthly temperature and precipitation statistics, including means, standard deviations, and cross-correlations.

(4) ForClim was initialized with the RCP4.5 and RCP8.5 scenarios, representing moderate and severe climate change impacts, respectively. These scenarios were derived from the CH2018 climate projections, which are based on EURO-CORDEX simulations containing 68 ensembles [6, 7]. For both RCP4.5 and RCP8.5, all ten available model ensembles at 12 km grid resolution were implemented in ForClim to capture inter-model variability. Subsequently, the simulation results were averaged across ensembles to create robust mean values.

(5) Swiss-wide soil data from Baltensweiler et al. [1] were processed to derive water holding capacity using the Rosetta pedotransfer model [17, 20]. Since the data contained gaps for the specific AOI, soil data for the entire forest district "Oberwald" were extracted instead. ForClim was initialized with a soil depth of 2000 mm.

2.1.5 Multi-criteria decision analysis

The Multi-Criteria Decision Analysis (MCDA) framework is based on Blattert et al. [3, 2] and Thrippleton et al. [18]. For this case study, 14 different indicators were selected and assigned to Biodiversity and the Ecosystem Services (BES) of recreation, carbon sequestration, and timber production (Tab. 1). The indicators were calculated based on the ForClim simulation output. Value and normalization functions were then applied to aggregate indicators into partial utilities for each BES group (Eq. 1) and an

overall utility (Eq. 2), using specific weights (Tab. 1). The overall utility ranges from 0 (lowest) to 1 (highest). The weighting of the overall utility (i.e., λ_a) was based on the management preferences of the local forester Stefan Haab, with a focus on timber production.

Table 1: Overview of BES and allocated indicators. The focus weights of BES groups (λ_a) represent the forester's objectives. Indicator specific weights (λ_i) derived from Blattert et al. [2]. Carbon sequestration consists of five compartments: above-below ground carbon, carbon in deadwood, carbon storage in harvested products (HWPs), substitution effects for energetic use, substitution effects for material use.

BES	λ_a	Indicator	λ_i
Biodiversity	0.2	Shannon index alpha	0.25
		Post-hoc index alpha	0.25
		Total deadwood volume ($m^3 ha^{-1}$)	0.25
		Number of habitat trees per ha (DBH > 70 cm)	0.25
Recreation	0.1	Mean height of 100 largest trees (per ha)	0.22
		Variation in tree size (Post-hoc index)	0.17
		Variation in tree species (Shannon index)	0.11
		Stand density index (SDI)	0.17
		Deadwood - harvest residue ($m^3 ha^{-1}$)	0.22
		Deadwood - natural mortality ($m^3 ha^{-1}$)	0.11
Carbon sequestration	0.1	Carbon sequestration ($tCha^{-1}$)	1
Timber production	0.6	Timber harvested ($m^3\ ha^{-1} yr^{-1}$)	0.8
		Productivity ($m^3\ ha^{-1} yr^{-1}$)	0.2

$$PU_{a,p,m,c} = \sum_{i \in I_a} \lambda_i u(x_{i,p,m,c}) \tag{1}$$

where:

- $PU_{a,p,m,c}$ = partial utility for BES group a in period p under management strategy m and climate scenario c
- I_a = set of indicators belonging to BES group a
- λ_i = weights for each indicator i
- $u(x_{i,p,m,c})$ = normalized utility for each individual indicator i within BES group a ($i \in I_a$)

$$OU_{p,m,c} = \sum_{a=1}^{A} \lambda_a PU_{a,p,m,c} \tag{2}$$

where:

- $OU_{p,m,c}$ = overall utility in period p under management strategy m and climate scenario c
- A = total number of BES groups
- λ_a = weights for each BES group

2.2 Results

2.2.1 Initial forest inventory based on LiDAR

For the Area of Interest (AOI: 3.7 ha), the forest inventory based on the LiDAR data contains 1585 trees, a basal area of 23.6 m^2/ha and a volume of 280.59 m^3/ha (Tab. 2). The main tree species detected are Norway spruce (*Picea abies*), followed by silver birch (*Betula pendula*) and silver fir (*Abies alba*), which are classified as small timber. Douglas fir (*Pseudotsuga menziesii*) and Scots pine (*Pinus sylvestris*) with larger DBH values can be classified as medium timber. The spatial distribution of trees over the AOI is illustrated in Fig. 5.

Table 2: LiDAR-based forest inventory results for the case study area (AOI: 3.7 ha). Tree volumes based on species-specific form factors [13].

Species	N	%	DBH (cm)				Height (m)				Basal area	Volume
			Mean	SD	Min	Max	Mean	SD	Min	Max	(m^2ha^{-1})	(m^3ha^{-1})
P. abies	888	56.0	24.3	8.2	7.5	70.0	23.1	5.3	3.6	40.0	12.40	147.24
B. pendula	209	13.2	21.9	8.4	8.8	48.2	20.4	5.7	4.0	32.7	2.44	24.27
A. alba	143	9.0	24.8	9.9	8.0	71.5	21.7	6.1	3.2	36.7	2.16	24.94
P. sylvestris	141	8.9	23.4	8.4	8.8	44.7	21.4	5.7	5.6	30.3	1.85	19.74
P. menziesii	72	4.5	38.2	11.5	19.4	75.0	31.9	5.1	18.3	41.1	2.43	36.25
A. pseudoplatanus	52	3.3	23.1	8.3	9.0	39.8	21.1	6.3	4.3	29.7	0.66	6.73
L. decidua	43	2.7	34.7	8.7	20.0	54.5	28.9	3.0	22.1	34.6	1.16	15.66
Q. robur	16	1.0	24.8	6.9	13.0	35.3	22.0	5.2	8.7	27.6	0.22	2.78
P. tremula	11	0.7	16.3	6.4	9.5	32.0	13.8	1.4	11.8	16.2	0.07	0.44
F. sylvatica	5	0.3	26.0	10.9	9.0	38.6	19.9	7.5	8.1	26.7	0.08	0.94
Q. petraea	4	0.3	34.4	7.3	28.7	44.1	28.0	1.8	26.0	30.1	0.10	1.51
C. betulus	1	0.1	20.0	n.a.	20.0	20.0	24.2	n.a.	24.2	24.2	0.01	0.09
Total	1585	100.0	24.8	9.3	7.5	75.0	22.9	6.0	3.2	41.1	23.61	280.59

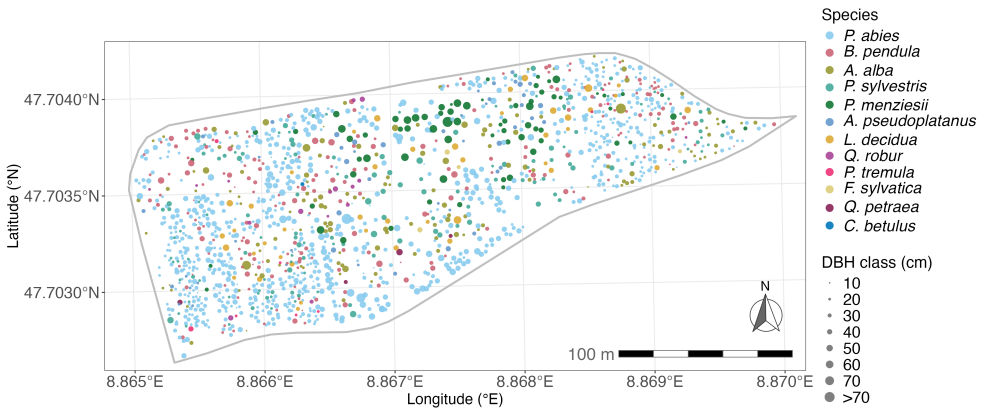

Figure 5: Spatial distribution of tree species and DBH classes for AOI (3.7 ha).

2.2.2 Tree Detection Rate (TDR)

The Tree Detection Rate (TDR) for the entire AOI is 75.6%, indicating that 512 trees are not detected by the segmentation algorithm (Tab. 3). Analysis of three sample areas within the AOI reveals substantial spatial variation in detection performance. Sample areas 1 and 2 achieve TDRs of approximately 90%, while sample area 3 shows a much lower performance with a TDR of 47.2%, accounting for 338 of the 512 missing trees and covering only 0.56 ha. Detection performance correlated inversely with tree density (measured in trees per hectare), with higher tree densities producing lower TDRs. The spatial distribution of successfully segmented and undetected trees (i.e. missing) across the three sample areas is illustrated in Fig. 6.

Table 3: Summary statistics of tree detection and segmentation by sample area (TDR = tree detection rate).

Sample area	Area (ha)	Total trees	Trees/ha	Segmented	Missing	TDR (%)
Sample area 1	1.38	864	625	744	120	86.1
Sample area 2	1.75	593	339	539	54	90.9
Sample area 3	0.56	640	1148	302	338	47.2
Total	3.69	2097	568	1585	512	75.6

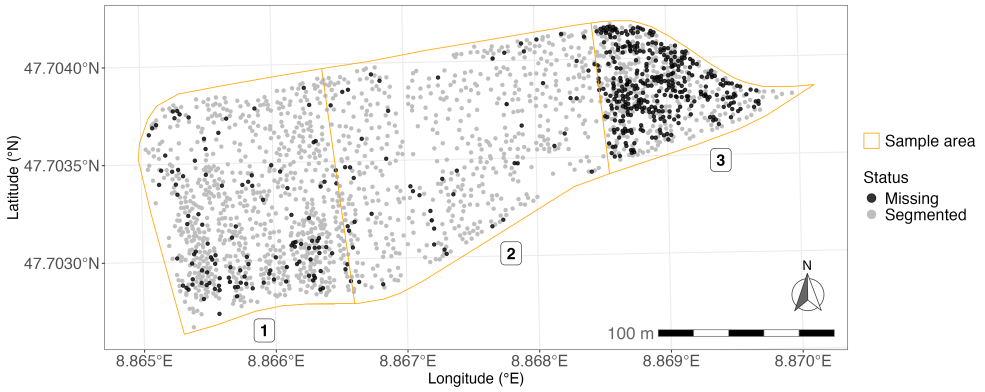

Figure 6: Distribution of segmented trees and undetected trees (i.e., missing trees) for three sample areas.

2.2.3 Simulated climate and management effects on basal area

The trajectory of basal area shows distinct patterns across management intensities and climate scenarios (Fig. 7). Under the historical climate (HIST) with no management intervention (NO), basal area steadily increases from approximately 23 m^2/ha to 44 m^2/ha over the simulation period, with Norway spruce (*Picea abies*) establishing clear dominance.

Under low-intensity management (LOW) with historical climate, harvesting begins when the stand approaches the basal area equilibrium target of 40 m^2/ha around 2070, stabilizing the basal area at this level. In contrast, high-intensity plentering (HIGH) maintains a stable basal area trajectory near 20 m^2/ha throughout the simulation period, as the equilibrium state is already achieved. This intensive management reduces

Norway spruce dominance and promotes a more diverse species composition, with increased proportions of silver fir (*Abies alba*), European beech (*Fagus sylvatica*), and other broadleaved species. Notably, Douglas fir (*Pseudotsuga menziesii*) proportions decrease under both LOW and HIGH management scenarios.

Under moderate climate change (RCP4.5), similar patterns emerge, though basal area accumulation in NO and LOW scenarios begins to slow after 2050. The LOW management scenario remains slightly below the 40 m^2/ha equilibrium target. The HIGH management scenario shows enhanced establishment of warm-adapted species, particularly sweet chestnut (*Castanea sativa*), oak species (*Quercus spp.*), and linden (*Tilia spp.*).

Severe climate change (RCP8.5) dramatically alters these trajectories. Both NO and LOW management scenarios experience substantial basal area decline after 2070, dropping from peak values of approximately 35 m^2/ha to below 30 m^2/ha by 2100. This decline is primarily driven by Norway spruce mortality, while the HIGH management scenario maintains relatively stable basal area with increased dominance of climate-adapted species.

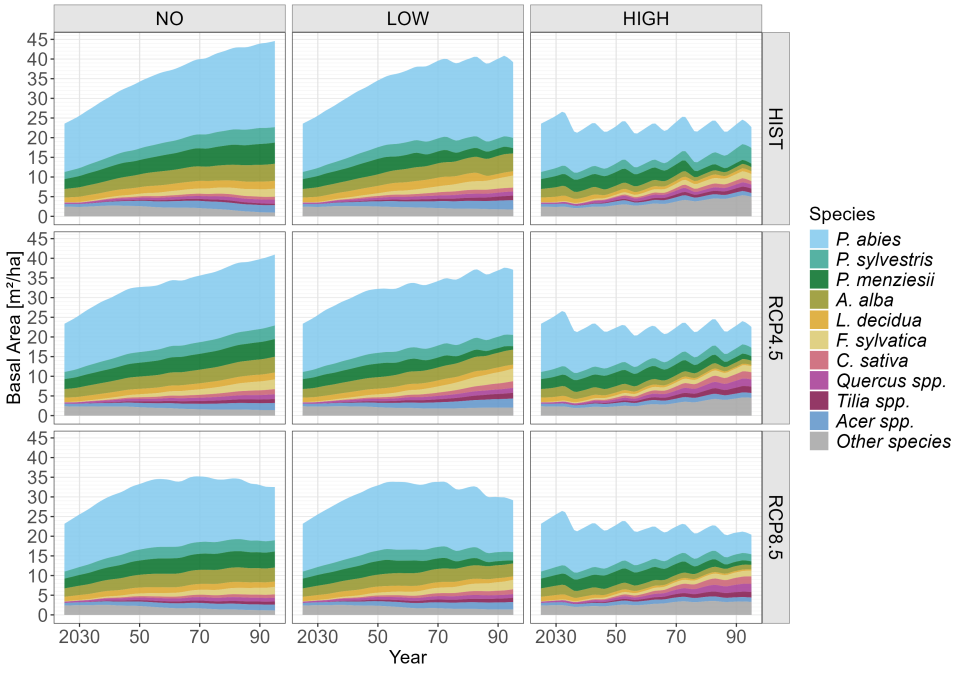

Figure 7: Basal area trajectories from 2025 to 2095 for management and climate scenarios, subdivided for relevant tree species. Maple (*Acer campestre, Acer platanoides, Acer pseudoplatanus*), linden (*Tilia cordata, Tilia platyphyllos*) and oak species (*Quercus petraea, Quercus pubescens, Quercus robur*) were aggregated at the genus level.

2.2.4 Simulated climate and management effects on productivity

Forest productivity, measured as annual increment (m^3/ha/year), varies substantially across management intensities and climate scenarios (Fig. 8). Under historical climate conditions (HIST), the LOW management scenario maintains the highest productivity throughout the simulation period, consistently exceeding 10 m^3/ha/year. The NO man-

agement scenario shows gradually declining productivity, falling from approximately 10 m^3/ha/year to below 9 m^3/ha/year by 2100. The HIGH management scenario exhibits the lowest but most stable productivity, maintaining approximately 8 m^3/ha/year throughout the simulation. Under HIGH management, Norway spruce increment decreases while Scots pine (*Pinus sylvestris*) shows increased growth, contributing to a shift in species productivity patterns.

Moderate climate change (RCP4.5) induces gradual productivity declines across all management scenarios. The LOW and NO management scenarios experience modest reductions starting around 2050, with productivity declining to approximately 9 m^3/ha/year by 2100. The HIGH management scenario shows greater resilience, maintaining relatively stable productivity around 7-8 m^3/ha/year. While Douglas fir (*Pseudotsuga menziesii*) contributes to productivity mid-simulation, it declines toward the end of the period, with warm-adapted broadleaved species becoming more important for maintaining productivity levels.

Severe climate change (RCP8.5) causes dramatic productivity losses across all management strategies. A sharp decline begins around 2050, with Norway spruce productivity collapsing substantially. By 2100, all management scenarios converge to similarly low productivity levels around 5-6 m^3/ha/year. The HIGH management scenario maintains greater diversity of climate-adapted species, including increased contributions from sweet chestnut (*Castanea sativa*), oak species (*Quercus spp.*), and other broadleaved species that partially offset the severe Norway spruce decline.

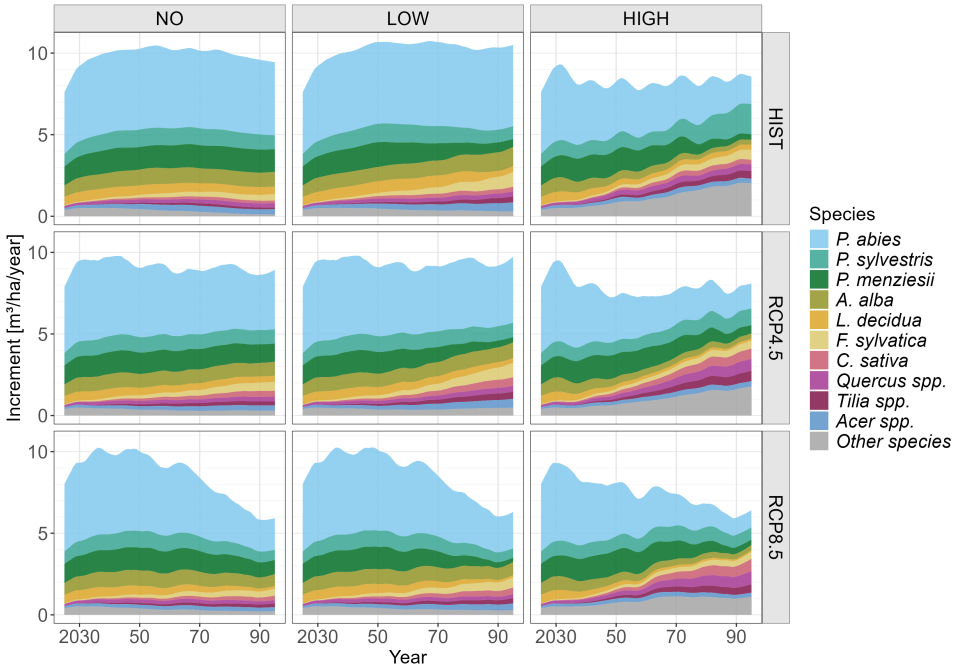

Figure 8: Productivity measured as increment ($m^3\ ha^{-1}\ year^{-1}$) from 2025 to 2095 for management and climate scenarios, subdivided by relevant tree species. Maple (*Acer campestre*, *A. platanoides*, *A. pseudoplatanus*), linden (*Tilia cordata*, *T. platyphyllos*), and oak species (*Quercus petraea*, *Q. pubescens*, *Q. robur*) were aggregated at the genus level.

2.2.5 MCDA: Aggregated partial and overall utility

The MCDA results, using focus weights favoring timber production (0.6), reveal distinct patterns across management strategies and climate scenarios (Fig. 9). Under historical climate (HIST), the HIGH management scenario achieves the highest overall utility score, driven primarily by its strong timber production performance. The LOW and NO management scenarios achieve progressively lower overall utilities. The NO scenario shows the highest partial utilities for biodiversity and recreation, but these contribute less to the overall score due to the timber-focused weighting scheme.

Climate change impacts alter these utility patterns while maintaining the relative ranking of management strategies. Under moderate climate change (RCP4.5), overall utility scores decrease across all scenarios, with HIGH management maintaining the highest score, followed by LOW and NO. The reduction is primarily driven by decreased timber production utilities across all management strategies as climate stress intensifies.

Severe climate change (RCP8.5) shows similar patterns with further utility reductions. HIGH management continues to achieve the highest overall utility, though timber production utilities continue to decline. Notably, biodiversity and recreation partial utilities remain relatively stable across all climate scenarios, showing minimal sensitivity to climate change regardless of management strategy. Carbon sequestration shows the highest partial utility under LOW management in historical climate but decreases substantially under climate change scenarios, with the strongest reductions occurring under RCP8.5. The HIGH management scenario reveals clear trade-offs: while maximizing timber production utility, it results in lower partial utilities for biodiversity, recreation, and carbon sequestration compared to NO and LOW management strategies.

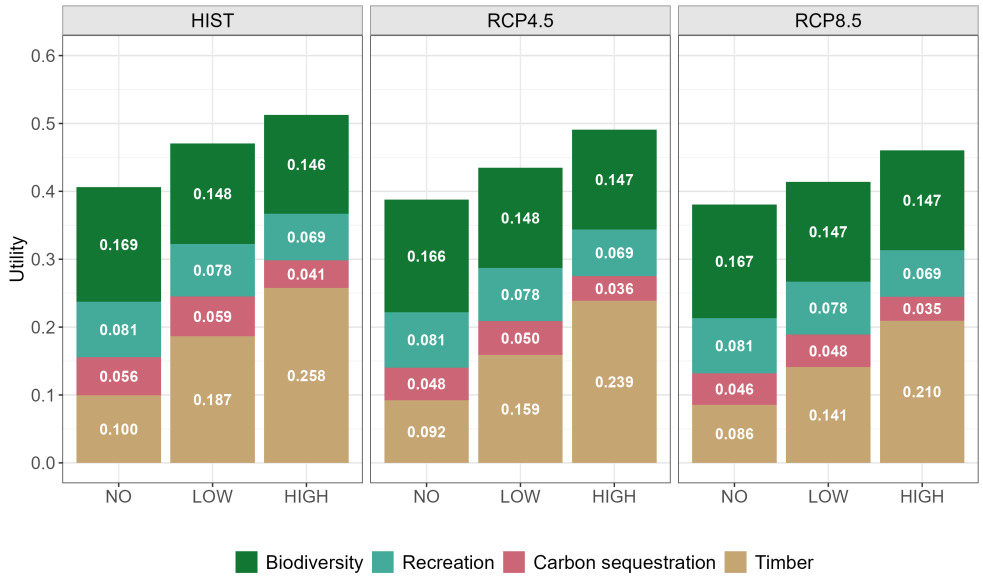

Figure 9: Overall utility with partial contribution from biodiversity, recreation, carbon sequestration and timber. Focus weighted scenario: timber 0.6, biodiversity 0.2, recreation 0.1, carbon sequestration 0.1.

2.3 Discussion

High-resolution LiDAR was successfully integrated into an existing DSS pipeline, addressing limitations in forest growth model initialization. Since traditional forest model often rely on coarse-resolution national forest inventory data, potentially misrepresenting local stand conditions.

The applied method successfully derives comprehensive forest inventory data from high-resolution ULS and TLS data. Point density mapping proved to be a suitable approach for validating DBH values. Tree species predictions using the deep learning model *DetailView* generally align with field observations. It correctly identifies the dominance of Norway spruce as small timber and Douglas fir and Scots pine as medium timber. However, silver birch abundance appears overestimated while European beech is underestimated. Final verification through manual tree inventory is pending.

The overall TDR of 75.6% achieved using *ForAINet* represents reasonable performance that exceeds TLS benchmarks reported by Kükenbrink et al. [12]. The significantly lower TDR in sample area 3 (47.2%) can be explained by its much higher tree density (1,148 trees/ha), which increases segmentation complexity [19]. Additionally, the TLS setup density in sample area 3 may have been insufficient (Fig. 2), likely causing occlusion effects. To ensure reliable segmentation in denser forests, a higher density of TLS setups should be targeted.

Given the time requirements, stationary TLS processing is not yet efficient enough for operational use. The method is labor-intensive, requires expensive equipment, and demands computationally intensive data processing to derive single-tree attributes. These operational limitations need to be addressed in future research to enable upscaling to multiple forest stands or management units.

3 Nordic DSS

3.1 Material and Methods

3.1.1 Study area

The test area for the trials is located in Evo, southern Finland Fig. 10. The area is used widely for remote sensing-based forestry research by University of Helsinki, University of Eastern Finland, and Finnish Geospatial Institute. Forests are a mixture of natural and commercially managed forests, and the age structure combines young sapling stands and old growth forests. The composition of the species consists of Scots pine (*Pinus sylvestris*), Norwegian spruce (*Picea abies*), and silver birch (*Betula pendula*). The area selected for scanning was 119 hectares in total, covering all species and stages of development of boreal forest that are used for commercial operations.

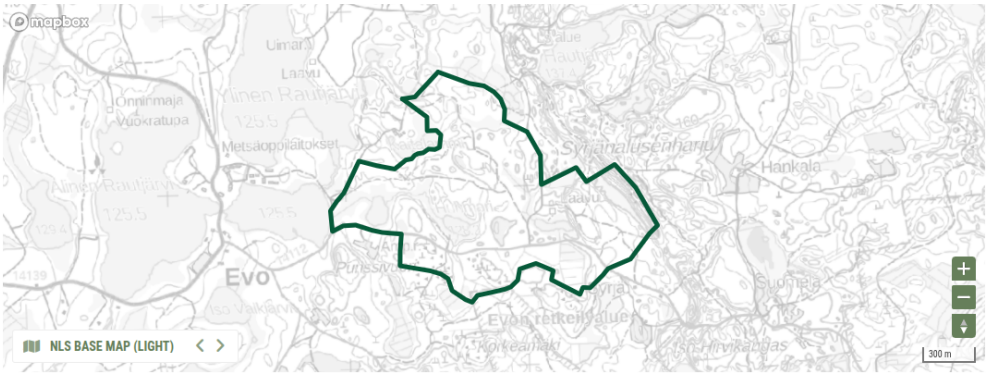

Figure 10: Location and borders of Evo research area.

3.1.2 LiDAR Data

Aerial data were collected using PreFor's in-house developed UAV-LiDAR payload. The LiDAR sensors employed were the Velodyne HDL-32e during the 2023 campaigns and the Hesai XT-32M2X during the 2025 campaigns. All datasets were post-processed with PreFor's proprietary cloud-based point cloud processing software. Data acquisition took place in May 2023 and June 2025 in Evo, Finland.

In addition, terrestrial data were collected using the University of Oxford's Frontier mobile mapping device mounted on a backpack. The integration of aerial and terrestrial datasets improved tree detection rates beneath the upper canopy, with particular benefits for identifying smaller trees in forest's with multiple storeys.

3.2 Results

3.2.1 Research area forest inventory

Forest inventory was calculated for the entire research area of 107 hectares using PreFor's proprietary cloud based software. In total 100.853 trees were detected with total volume of 21.922 cubic meters. Forest inventory can be presented in web based user interface in tree level (Fig. 11).

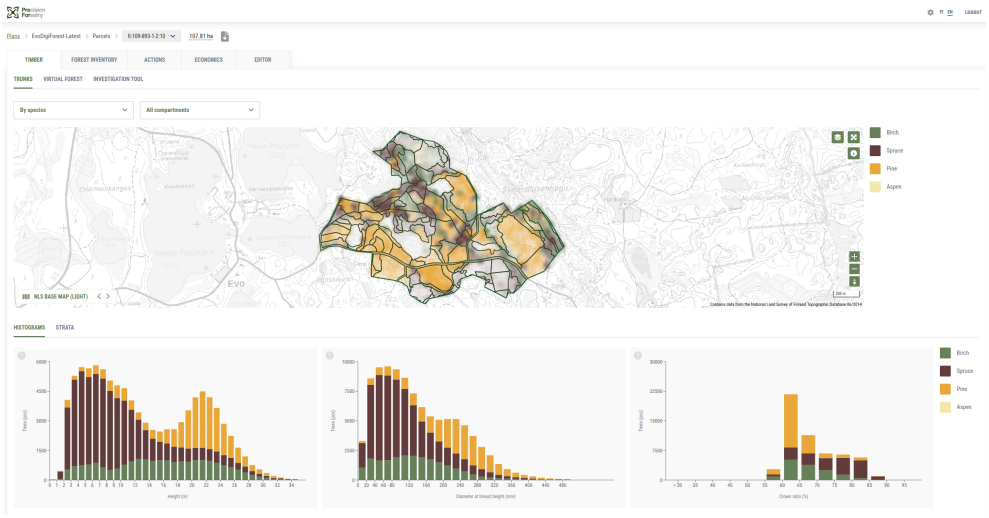

Figure 11: Screenshot from PreFor's browser based user interface.

A biodiversity-related indicator was incorporated into the system by using tree species and size data to calculate the Shannon alpha index, the Post-hoc alpha index, and the number of habitat trees. Habitat trees were defined as those exceeding 50 cm in diameter, in line with Nordic conditions. Each variable was normalized against the maximum value observed in individual tree-level data, gridded into approximately 20 × 20 m units. After normalization, equal weights were assigned to each variable, and their sum was used to derive the biodiversity index. This index was further aggregated to the stand level, where the average value was applied.

In PreFor's system, biodiversity is expressed as local variation within narrowly defined areas and is not intended for comparison across different forest parcels. Instead, the identification of local biodiversity hotspots supports logging operation planning by highlighting areas of high ecological value that should remain undisturbed. The values of the biodiversity index are presented in (Fig. 12) in the research area, Evo.

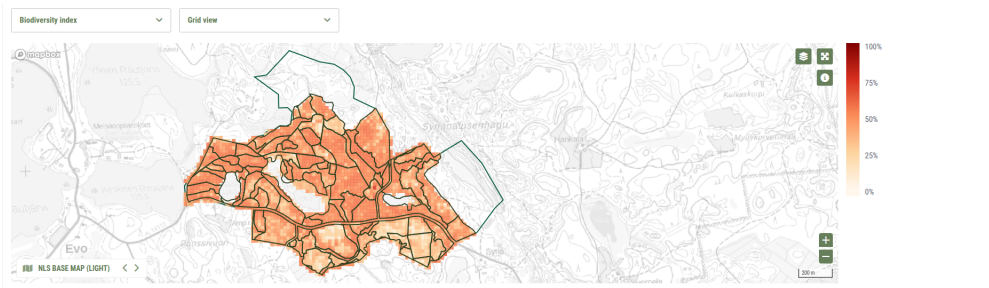

Figure 12: Screenshot from PreFor's browser based user interface presenting biodiversity index in Evo.

In addition to the main forest inventory conducted at the Evo test site, an independent experiment was carried out in Porvoo, Finland, to evaluate inventory accuracy under different data acquisition conditions. The test area in Porvoo was the same site previously used for testing the SAHA robot.

Based on field reference measurements, the tree detection rate was significantly

improved by integrating terrestrial point cloud data with aerial point cloud data. When using only aerial data, the detection rate reached 84

The accuracies derived from three field plots at the Porvoo site, in terms of basal area and volume, are presented in Table 4.

Table 4: Summary of the inventory accuracy in SAHA test site in Porvoo, Finland

Data	Attribute	Bias-%	RMSE-%
UAV	Basal area	-4	9.2
Combined	Basal area	4.8	6.1
UAV	Volume	-4.4	8
Combined	Volume	1.5	2.9

3.3 Discussion

High-density airborne and terrestrial laser scanning can be used to accurately capture spatial patterns derived from individual tree-level data. This detailed view of the forest provides insights into the processes influencing forest resource use, which can be effectively interpreted by experienced users through the web-based software. The platform is also designed to be easily accessible for a wide range of stakeholders.

Combining individual tree data with growth models that incorporate spatial competition indices improves the accuracy of projecting forest development under alternative future scenarios. This approach also supports tree-level planning of upcoming thinning operations, providing benefits for both forest owners and machine operators. It was also proven that utilizing terrestrial point cloud data together with aerial point cloud data for producing inventory, has improved the accuracy significantly, which makes the inventory better suitable for the market.

4 Outlook

The Central European DSS framework is suitable for the integration of LiDAR-based forest inventory. Current research focuses on integrating economic aspects within the DSS, such as wood revenue. This adds another important variable for the decision-making process and allows illustration of financial losses due to climate change effects or when promoting other ecosystem services, such as biodiversity or recreation. In addition, a publication is in progress that investigates the added value of high-resolution LiDAR data for the initialization. For this, the sensitivity along the DSS pipeline to the initial stand resolution will be analyzed.

The Nordic DSS is designed primarily to support practical decision-making for planning logging operations, rather than focusing on large-scale future projections. The initial idea was to incorporate multi-attribute decision making into the decision support system, but as the end-user of the system is not going to be decision maker, logic was changed to just support logging operation planning. System integrates individual tree-level data with enriched datasets to assist in evaluating both wood production and non-wood ecosystem services. The system is expected to be applied in

commercial operations starting in 2026. In the first phase, planning will be carried out manually by experienced operators, ensuring that ecosystem services are considered alongside wood production. In the next phase, planning will be fully automated, enabling larger-scale operations.

References

[1] Andri Baltensweiler et al. *Soil property maps for the Swiss forest*. 2024. DOI: http://dx.doi.org/10.16904/envidat.484. URL: https://www.envidat.ch/dataset/soil-property-maps-for-the-swiss-forest.

[2] Clemens Blattert et al. "Managing European Alpine forests with close-to-nature forestry to improve climate change mitigation and multifunctionality". In: *Ecological Indicators* 165 (Aug. 2024), p. 112154. ISSN: 1470-160X. DOI: 10.1016/j.ecolind.2024.112154. URL: https://www.sciencedirect.com/science/article/pii/S1470160X24006113 (visited on 12/11/2024).

[3] Clemens Blattert et al. "Segregated versus integrated biodiversity conservation: Value-based ecosystem service assessment under varying forest management strategies in a Swiss case study". en. In: *Ecological Indicators* 95 (Dec. 2018), pp. 751–764. ISSN: 1470160X. DOI: 10.1016/j.ecolind.2018.08.016. URL: https://linkinghub.elsevier.com/retrieve/pii/S1470160X18306150 (visited on 04/02/2025).

[4] Harald Bugmann. "A Review of Forest Gap Models". en. In: *Climatic Change* 51.3 (Dec. 2001), pp. 259–305. ISSN: 1573-1480. DOI: 10.1023/A:1012525626267. URL: https://doi.org/10.1023/A:1012525626267 (visited on 06/19/2025).

[5] Harald Bugmann. "A Simplified Forest Model to Study Species Composition Along Climate Gradients". en. In: *Ecology* 77.7 (Oct. 1996), pp. 2055–2074. ISSN: 0012-9658, 1939-9170. DOI: 10.2307/2265700. URL: https://esajournals.onlinelibrary.wiley.com/doi/10.2307/2265700 (visited on 04/21/2025).

[6] CH2018. *CH2018 – Climate Scenarios for Switzerland*. Technical Report. ISBN: 978-3-9525031-4-0. Zurich: National Centre for Climate Services, 2018, p. 271.

[7] I Feigenwinter and S Kotlarski. *Exploring quantile mapping as a tool to produce user-tailored climate scenarios for Switzerland*. Tech. rep. 2018.

[8] Rico Fischer et al. "Perspectives for forest modeling to improve the representation of drought-related tree mortality". In: (Apr. 2025), pp. 55–69. DOI: 10.5073/JfK.2025.02.05.

[9] Julian Frey and Zoe Schindler. *JulFrey/CspStandSegmentation: Single tree segmentation from terestrial LiDAR forest scans*. Nov. 2024. DOI: 10.5281/zenodo.14204460. URL: https://zenodo.org/records/14204460 (visited on 04/30/2025).

[10] Julian Frey and Zoe Schindler. *JulFrey/DetailView: DetailView model for tree species classification based on single tree LiDAR data*. Nov. 2024. DOI: 10.5281/zenodo.14204431. URL: https://zenodo.org/records/14204431 (visited on 04/30/2025).

[11] Ulrike Hiltner and Gina Marano. *rforclim: Collection of useful functions to parameterize and run the forest model ForClim for both versions 4.0.1. and 4.1. and analyze its simulation results*. 2024. DOI: 10.3929/ethz-a-000946508. URL: https://gitlab.ethz.ch/ites-fe/rforclim/.

[12] Daniel Kükenbrink et al. "Benchmarking laser scanning and terrestrial photogrammetry to extract forest inventory parameters in a complex temperate forest". en. In: *International Journal of Applied Earth Observation and Geoinformation* 113 (Sept. 2022), p. 102999. ISSN: 15698432. DOI: 10.1016/j.jag.2022.102999. URL: https://linkinghub.elsevier.com/retrieve/pii/S1569843222001881 (visited on 06/11/2025).

[13] K.-W. Lockow. "Formzahlen, Formzahlfunktionen und Formzahltabellen des Einzelbaumes". In: *Waldbestandsmessung – Stichprobenverfahren – Wachstumsmodellierung*. Section: 8. Springer-Verlag GmbH, 2022, pp. 203–240. DOI: 10.1007/978-3-662-63061-7_8.

[14] Gina Marano et al. *Predicting Drought-Induced Tree Mortality in Swiss Beech Forests Hinges Upon Predisposing and Inciting Factors*. Dec. 2024. DOI: 10.2139/ssrn.5077989.

[15] MeteoSchweiz. *Startseite - MeteoSchweiz*. de. 2024. URL: https://www.meteoschweiz.admin.ch/ (visited on 06/01/2025).

[16] Stefano Puliti et al. "Benchmarking tree species classification from proximally sensed laser scanning data: Introducing the FOR-species20K dataset". en. In: *Methods in Ecology and Evolution* 16.4 (2025), pp. 801–818. ISSN: 2041-210X. DOI: 10.1111/2041-210X.14503. URL: https://onlinelibrary.wiley.com/doi/abs/10.1111/2041-210X.14503 (visited on 04/21/2025).

[17] Marcel G. Schaap, Feike J. Leij, and Martinus Th. van Genuchten. "rosetta: a computer program for estimating soil hydraulic parameters with hierarchical pedotransfer functions". In: *Journal of Hydrology* 251.3 (Oct. 2001), pp. 163–176. ISSN: 0022-1694. DOI: 10.1016/S0022-1694(01)00466-8. URL: https://www.sciencedirect.com/science/article/pii/S0022169401004668 (visited on 05/01/2025).

[18] Timothy Thrippleton et al. "A Multi-Criteria Decision Support System for Strategic Planning at the Swiss Forest Enterprise Level: Coping With Climate Change and Shifting Demands in Ecosystem Service Provisioning". English. In: *Frontiers in Forests and Global Change* 4 (Aug. 2021). Publisher: Frontiers. ISSN: 2624-893X. DOI: 10.3389/ffgc.2021.693020. URL: https://www.frontiersin.org/journals/forests-and-global-change/articles/10.3389/ffgc.2021.693020/full (visited on 11/08/2024).

[19] Binbin Xiang et al. "Automated forest inventory: Analysis of high-density airborne LiDAR point clouds with 3D deep learning". en. In: *Remote Sensing of Environment* 305 (May 2024), p. 114078. ISSN: 00344257. DOI: 10.1016/j.rse.2024.114078. URL: https://linkinghub.elsevier.com/retrieve/pii/S0034425724000890 (visited on 03/07/2025).

[20] Yonggen Zhang and Marcel G. Schaap. "Weighted recalibration of the Rosetta pedotransfer model with improved estimates of hydraulic parameter distributions and summary statistics (Rosetta3)". In: *Journal of Hydrology* 547 (Apr. 2017), pp. 39–53. ISSN: 0022-1694. DOI: 10.1016/j.jhydrol.2017.01.004. URL: https://www.sciencedirect.com/science/article/pii/S0022169417300057 (visited on 05/01/2025).